



Pressure-induced structural evolution and amorphization in $\text{Eu}_3\text{Ga}_5\text{O}_{12}$

C. L. Lin, Y. C. Li, X. D. Li, R. Li, J. F. Lin et al.

Citation: *J. Appl. Phys.* **114**, 163521 (2013); doi: 10.1063/1.4827836

View online: <http://dx.doi.org/10.1063/1.4827836>

View Table of Contents: <http://jap.aip.org/resource/1/JAPIAU/v114/i16>

Published by the [AIP Publishing LLC](#).

Additional information on *J. Appl. Phys.*

Journal Homepage: <http://jap.aip.org/>

Journal Information: http://jap.aip.org/about/about_the_journal

Top downloads: http://jap.aip.org/features/most_downloaded

Information for Authors: <http://jap.aip.org/authors>



Re-register for Table of Content Alerts

Create a profile.



Sign up today!



Pressure-induced structural evolution and amorphization in $\text{Eu}_3\text{Ga}_5\text{O}_{12}$

C. L. Lin,¹ Y. C. Li,¹ X. D. Li,¹ R. Li,¹ J. F. Lin,² and J. Liu^{1,a)}

¹*Institute of High Energy Physics, Beijing Synchrotron Radiation Facility, Chinese Academy of Sciences, Beijing 100049, China*

²*Department of Geological Sciences, Jackson School of Geosciences, The University of Texas at Austin, Austin, Texas 78712, USA*

(Received 24 August 2013; accepted 14 October 2013; published online 30 October 2013)

Crystal structural evolution of europium gallium garnet ($\text{Eu}_3\text{Ga}_5\text{O}_{12}$; EGG) has been investigated by a combination of synchrotron x-ray diffraction, Raman scattering, and photoluminescence spectroscopy in a high-pressure diamond anvil cell. The cubic garnet EGG mostly collapses into an amorphous state upon compression to 85 GPa at room temperature. High-pressure Raman and photoluminescence spectra indicate that the amorphization process is related to the interaction and deformation of the tetrahedra GaO_4 and octahedra GaO_6 under compression, leading to the increase of the asymmetry of the local oxygen environment around the Eu^{3+} site with increasing pressures. The amorphization of EGG is associated with the overlapping of the tetrahedra and octahedra and the increase of the average coordination numbers of the Ga^{3+} ions in the amorphous state. X-ray diffraction spectra of EGG taken from a laser-heated diamond anvil cell demonstrate that the pressure-induced garnet-to-amorphous transition could result from the kinetic hindrance of a crystal-to-crystal phase transition at room temperature, rather than the decomposition reported earlier. © 2013 AIP Publishing LLC. [<http://dx.doi.org/10.1063/1.4827836>]

I. INTRODUCTION

The pressure-induced crystalline-to-amorphous transformation in the solid state has been the focus of intense study recently and has been observed in many materials^{1–5} since the amorphization of the solid H_2O was found at 1 GPa and 77 K.⁶ Specifically, the pressure-induced amorphization (PIA) has been observed in the rare earth element (REE) garnets.^{7,8} It has been reported that $\text{Gd}_3\text{Sc}_2\text{Ga}_3\text{O}_{12}$ (GSGG), $\text{Gd}_3\text{Ga}_5\text{O}_{12}$ (GGG), and $\text{Y}_3\text{Fe}_5\text{O}_{12}$ (YIG) transform to an amorphous state at 58 GPa, 84 GPa, and 50 GPa,^{7,8} respectively. The PIA transition in the REE garnets is shown to be irreversible. Because REE garnets doped with different REE elements have fascinating optical luminescent properties, which could serve as laser materials and new optical pressure sensors,^{9–16} understanding the structural evolution, thermodynamics, and driving mechanism of the crystalline-amorphous transformation is of great interest both from the fundamental and application points of view. However, few studies are focused on the structural change of the REE garnets to demonstrate the amorphization process in these systems.

REE garnets with the chemical formula $\text{R}_3\text{B}_2\text{C}_3\text{O}_{12}$, where R, B, and C denote the dodecahedral, octahedral, and tetrahedral sites in the lattice, respectively, have a cubic structure with a space group $Ia\bar{3}d$ and eight formula units in the unit cell. In the cubic structure, the R site is occupied by REE cations, while the B and C sites are occupied by Al^{3+} , Ga^{3+} , Fe^{3+} , or Sc^{3+} cations. The octahedra and tetrahedra form three-dimensional corner-sharing network in which each oxygen atom is shared by two dodecahedra, one tetrahedron, and one octahedron (Fig. 1). Similar to the reported PIA transitions in the REE

garnets, a number of the network-structured compounds such as ZrW_2O_8 ,³ ZrMo_2O_8 ,¹⁷ $\text{Sc}_2(\text{MoO}_4)_3$,¹⁸ $\text{Sc}_2(\text{WO}_4)_3$,¹⁹ $\text{Eu}_2(\text{MoO}_4)_3$,⁵ $\text{Dy}_2\text{Mo}_4\text{O}_{12}$,⁴ and ZrV_2O_7 ²⁰ are also observed to undergo crystalline-to-amorphous transitions at high pressures. Previous theoretical and experimental results provide evidence on the distortion and tilting of the tetrahedra as well as an increase of the cation coordination number in the amorphization of these network-structured compounds.^{3,5,17,21,22} It has been found that their transition pressures (<10 GPa) are systematically lower than that of the REE garnets (>50 GPa), suggesting a strong influence of the pressure-induced changes of the local oxygen environment around the R site on the amorphization process. Therefore, studying the structural changes of the REE garnets, such as $\text{Eu}_3\text{Ga}_5\text{O}_{12}$, can provide new insights into the underlying mechanisms of amorphization in the network-structured compounds.

A number of mechanisms including chemical decomposition and kinetic hindrance have been proposed to explain the pressure-induced amorphization in various materials.^{1,4,7,23–25} The decomposition process was reported in the YIG and $\text{Y}_3\text{Al}_5\text{O}_{12}$ (YAG) garnets that were decomposed to $3\text{YFeO}_3 + \text{Fe}_2\text{O}_3$ and $3\text{YAlO}_3 + \text{Al}_2\text{O}_3$ at high pressure and high temperature (P - T) conditions.²⁶ Different from the decomposition scenario, x-ray diffraction results from the laser-heated DAC experiments show that amorphous GGG and YIG transformed to a single cubic or orthorhombic perovskite structure at high P - T conditions.^{27,28} Additionally, we observed the garnet-to-perovskite phase transition in GSGG at 24 GPa and 1500–2000 K in our previous work,²⁹ rather than the decomposition of GSGG. It seems that the kinetic hindrance of the equilibrium phase transitions leads to the amorphization of the REE garnets under high pressures. Additionally, Gavriluk *et al.*⁸ concluded that the local atomic structure in the

^{a)}Author to whom correspondence should be addressed. Electronic mail: liuj@ihep.ac.cn

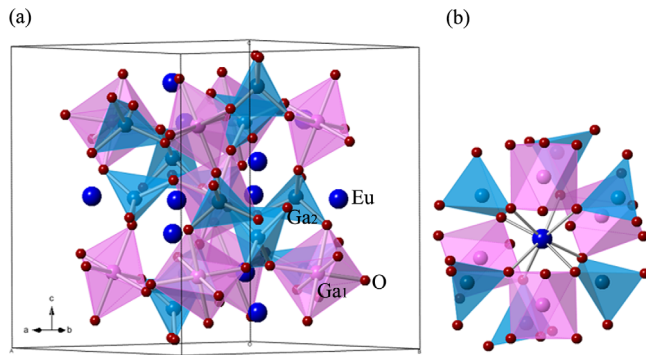


FIG. 1. The crystal structure of the EGG garnet, (a) shows one crystal unit cell, and (b) depicts part of the unit cell in which the Eu^{3+} ion lies between the octahedra and tetrahedra. In the cubic structure, Ga_1^{3+} occupies the octahedral site at the $(0, 0, 0)$ position, Ga_2^{3+} occupies the tetrahedral site with $(3/8, 0, 1/4)$ coordinate, and Eu^{3+} is at the dodecahedral site with the $(1/8, 0, 1/4)$ coordinate, respectively. Oxygen has the general coordinate (x, y, z) .

pressure-induced amorphous YIG consists of the FeO_6 octahedral complexes with an overall $\text{Y}_3\text{Fe}_5\text{O}_{12}$ formula from the x-ray diffraction patterns, further ruling out the probability of decomposition.

In order to decipher the PIA process in REE garnets, we have studied the crystal structural evolution and amorphization of europium gallium garnets ($\text{Eu}_3\text{Ga}_5\text{O}_{12}$; EGG) under high pressures using synchrotron x-ray diffraction, Raman scattering, and photoluminescence spectroscopy. Analyses of the x-ray diffraction spectra reveal variations of the cationic sublattice with elevated pressures. Raman spectra of EGG are used to investigate pressure-induced evolution of the octahedral-tetrahedral network via variations of the phonon vibrational mode, while the fluorescence spectroscopy of the Eu^{3+} ions in EGG can provide information about the pressure-induced variation of the local oxygen environment surrounding the dodecahedral site, which is connected to the change of the octahedra and tetrahedra. Consequently, the combination of these techniques can provide new insight into the structural change and the amorphization process of the REE garnets. Additionally, the discussion of the thermodynamics and driving mechanism of the crystalline-to-amorphous transition is presented.

II. EXPERIMENTAL DETAIL

Polycrystalline EGG starting samples were synthesized using the standard solid-state reaction technique.³⁰ X-ray diffraction and Raman scattering analyses of the synthesized sample confirmed that it has a pure single phase in the cubic

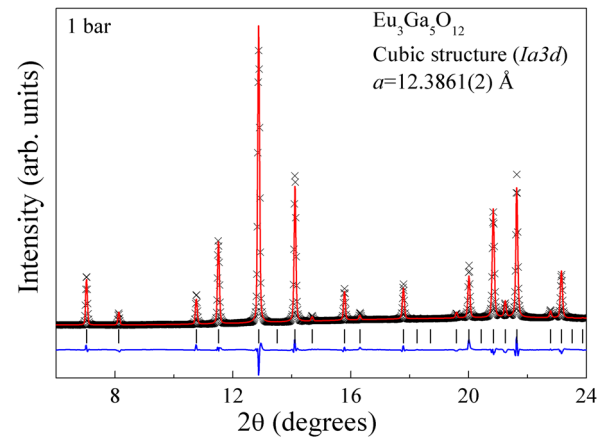


FIG. 2. Representative x-ray diffraction pattern of $\text{Eu}_3\text{Ga}_5\text{O}_{12}$ (EGG) with the Rietveld refinement at ambient conditions.

garnet structure with a space group $Ia\bar{3}d$. Figure 2 shows the Rietveld refinement of the x-ray diffraction pattern at ambient conditions with the lattice parameter (a) of $12.3861(2)$ Å. The oxygen atom has the general coordinate $(0.0259(4), 0.0595(5), 0.6570(6))$.

High-pressure x-ray diffraction experiments were performed using a pair of diamond anvils (DAC) with $150 \mu\text{m}$ or $300 \mu\text{m}$ culet sizes. In the first run, the sample was mixed with Pt which served as the pressure calibrant,³¹ while NaCl was used as pressure transmitting medium. The sample was compressed to ~ 85 GPa and observed to undergo crystalline-amorphous transition. In the second run, a disk of the sample without Pt was loaded into a sample hole with neon as the pressure transmitting medium and ruby spheres serving as pressure calibrants.³² In the third run, the powder sample was mixed with $\sim 8\%$ Pt which served as the pressure calibration and laser absorber. The argon was cryogenically loaded into the sample chamber as a pressure medium and thermal insulator. The sample was compressed to ~ 24 GPa and was laser-heated to 1500–2000 K. The experimental conditions and purposes were summarized in Table I.

In situ high-pressure angle dispersive x-ray diffraction experiments were conducted at the 4W2 beamline of the Beijing Synchrotron Radiation Facility (BSRF) with a wavelength of 0.6199 Å and a beam size of approximately $26 \times 8 \mu\text{m}^2$ (FWHM). X-ray diffraction patterns were collected using an image plate detector (MAR345), and were integrated using the Fit2D software package.³³ Integrated x-ray diffraction spectra were further analyzed for refined lattice parameters using the GSAS + EXPGUI program.³⁴

TABLE I. Experimental conditions. Room temperature: RT; Photoluminescence: PL.

Method	High-pressure XRD			Raman	PL
	Run 1	Run 2	Run 3		
Conditions					
Temperature	RT	RT	1500–2000 K	RT	RT
Medium	NaCl	Ne	Ar	Ne	Ne
Calibration	Pt	Ruby	Ruby	Ruby	Ruby
Pressure range (GPa)	0–85	0–47	0–24	0–68	0–68
Experimental purpose	Amorphization	Equation of state	Garnet-to-orthorhombic transition	Variation of phonon mode	Change of oxygen environment around Eu^{3+}

The high-pressure Raman and photoluminescence (PL) experiments were performed in the symmetric DAC with a pair of diamond anvils having a culet size of 300 μm . A powder sample disk of $\sim 30 \mu\text{m}$ thick was loaded into a sample chamber in a pre-indented Re gasket, together with ruby chips for pressure measurements.³² To provide a quasihydrostatic environment, neon was loaded into the sample chamber as the pressure transmitting medium using a gas loading system at BSRF-4W2. High-pressure and room-temperature luminescence and Raman spectra were collected with a confocal laser micro-Raman spectrometer. An Ar⁺ laser with a 488 nm line was used as the excitation laser source that focused to a spot size of 2 μm . Additionally, the 532 nm excited line was used to confirm that the luminescence spectra are not related to the excitation source.

III. RESULTS

A. X-ray diffraction

Upon compression, the diffraction peaks of EGG became broadened and shifted to higher angles, though EGG remained in the cubic garnet structure up to 75 GPa (Fig. 3). At 75 GPa, the diffraction peaks started to collapse into one broad peak at $2\theta = 14^\circ$, indicating the loss of the long-range order and onset of the amorphous state. EGG mostly became amorphous at 85 GPa.

Distinctly different diffraction peaks were observed after EGG was laser-heated to 1500–2000 K at ~ 24 GPa (Fig. 4), suggesting the occurrence of an intermediate phase between garnet and an amorphous state. According to the diffraction pattern, small amounts of the garnet phase

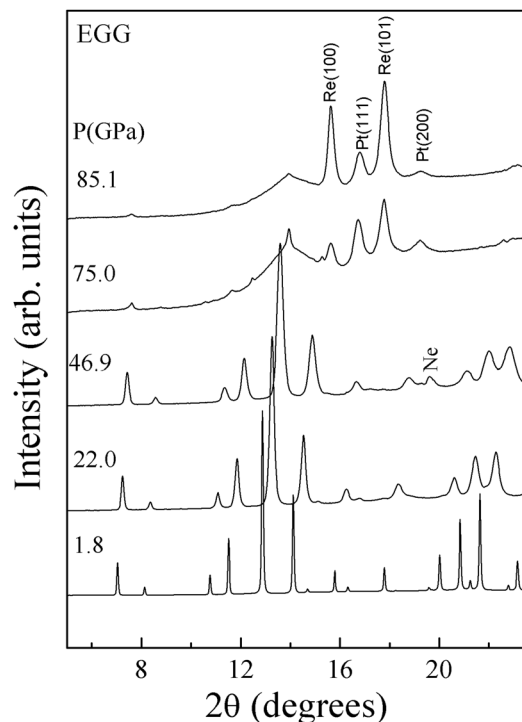


FIG. 3. Representative angle-dispersive x-ray diffraction patterns (wavelength $\lambda = 0.6199 \text{ \AA}$) of EGG at high pressures. The patterns above 50 GPa were collected in the first run mixed with Pt, while the spectra below 50 GPa were collected in the second run without Pt.

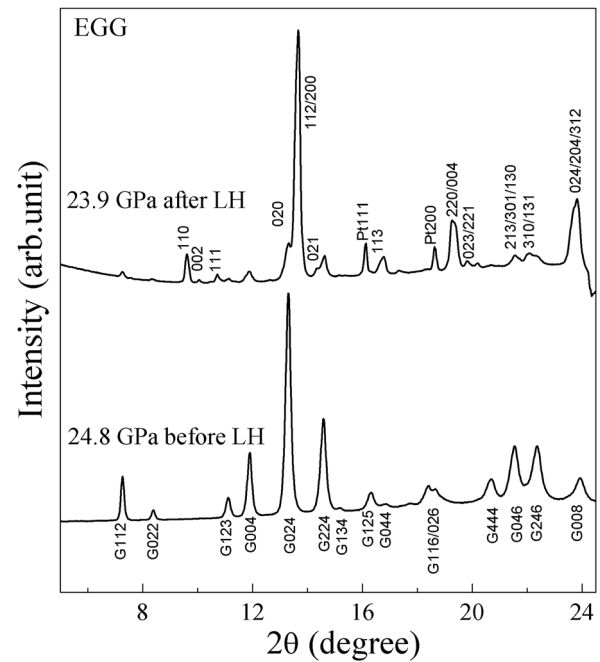


FIG. 4. Comparison of the x-ray diffraction patterns before and after laser-heating the EGG garnet. The bottom spectrum represents the x-ray diffraction of the cubic garnet phase, and the top shows the high-pressure orthorhombic phase after laser-heating.

remained in the laser-heating experiment (Fig. 4). The diffraction patterns of EGG after laser heating did not show the diffraction peaks of Ga_2O_3 , ruling out the occurrence of the decomposed mixtures of $3\text{GdGaO}_3 + \text{Ga}_2\text{O}_3$. Using the program *Dicvol*,³⁵ the new diffraction peaks can be well indexed into an orthorhombic phase with the space group *Pbnm*. Furthermore, the diffraction pattern of the intermediate phase for EGG is similar to that of the high-pressure orthorhombic perovskite structure of GSGG observed at ~ 24 GPa and 1500–2000 K,²⁹ suggesting that EGG undergoes the garnet-orthorhombic phase transition at the high *P-T* conditions. Based on the stoichiometry, the orthorhombic perovskite phase should have the chemical formula $\text{Eu}_{0.75}\text{Ga}_{0.25}\text{GaO}_3$ and can be quenched to ambient pressure, which is in agreement with GSGG.²⁹

Figure 5 shows the pressure dependence of the unit cell volume per formula ($\text{Eu}_3\text{Ga}_5\text{O}_{12}$) and the distance between the tetrahedra, octahedra, and dodecahedra. The pressure-volume (*P-V*) curve and distance of the nearest adjacent cations decrease monotonously with increasing pressure. The *P-V* curve of the garnet phase is fitted using the third Birch-Murnaghan equation of state (EoS),³⁶ yielding a bulk modulus $B_0 = 177(3)$ GPa, a pressure derivative of the bulk modulus $B'_0 = 5.4(2)$, and an ambient-condition volume $V_0 = 237.7(2) \text{ \AA}^3$. When B'_0 is fixed to 4.0, the bulk modulus, B_0 is 201(2) GPa with $V_0 = 236.9(2) \text{ \AA}^3$.

B. Photoluminescence spectroscopy

In garnet EGG, the Eu^{3+} ion occupies the dodecahedral site with D_2 symmetry. The energy levels of Eu^{3+} ($4f^6$) are split by the ligand field surrounding the Eu^{3+} ion. Figure 6 shows the selected photoluminescence spectra (PL) of Eu^{3+} in EGG at various pressures, related to the transitions

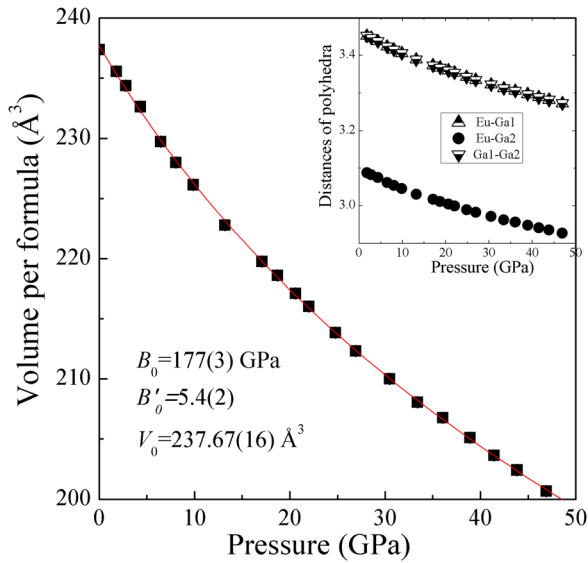


FIG. 5. Experimental P-V data of EGG. The inset is pressure dependence of the distances between nearest polyhedra (dodecahedra, octahedra, and tetrahedra).

from the excited state 5D_0 to the ground state multiplets 7F_J ($J = 1, 2$). The PL spectrum at ambient pressure is similar to the absorption spectrum of EGG and the fluorescence spectrum of $\text{Eu}^{3+}:\text{Gd}_3\text{Ga}_5\text{O}_{12}$.^{37,38} At ambient conditions, three lines for the ${}^5D_0 \rightarrow {}^7F_1$ transitions were observed, suggesting the complete removal of the degeneracy. Upon compression, the band at 16824 cm^{-1} (labeled as R3 in Fig. 6(b)) shifted to high energy, contrary to the red shift of the other two high-energy bands (labeled as R1 and R2 in Fig. 6(b)). The R1 and R2 bands merged into one at 4.4 GPa, and the R1 band merges with R3 at 10.3 GPa.

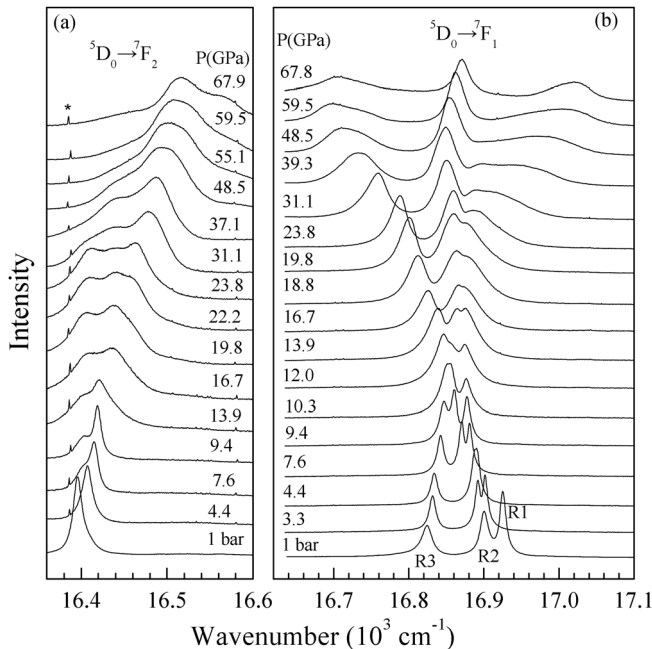


FIG. 6. Characteristic fluorescence spectra for the ${}^5D_0 \rightarrow {}^7F_J$ ($J = 1, 2$) transition of Eu^{3+} in $\text{Eu}_3\text{Ga}_5\text{O}_{12}$ at high pressures. The sharp peak at 16385 cm^{-1} marked with * represents the laser line.

A new emission band corresponding to the ${}^5D_0 \rightarrow {}^7F_2$ transition appeared at 7.6 GPa (Fig. 6(a)), and the relative intensity grew with increasing pressure. At 22.2 GPa, another new Stark component of the ${}^5D_0 \rightarrow {}^7F_2$ transition emerged. Additionally, the significant asymmetric broadening of the Stark splitting of the ${}^5D_0 \rightarrow {}^7F_1$ ($J = 1, 2$) transition was observed above 10 GPa. It is well-known that a number of factors, such as the nonhydrostatic pressure effect, variations of strength, and asymmetry of the crystal field in a free REE ion, can lead to the splitting and broadening of the Stark levels. In our experiments, neon was used as pressure transmitting medium and the hydrostatic pressure condition on the sample was revealed by well separated and individually resolved ruby lines, ruling out the nonhydrostatic effect on the Stark splitting and broadening. Therefore, it is conceivable that the variation of the crystal field around the dodecahedral site is the main factor for the Stark splitting and broadening.

The ${}^5D_0 \rightarrow {}^7F_2$ transition is electric dipole allowed and its intensity is sensitive to the local environment of the Eu^{3+} ion, whereas the ${}^5D_0 \rightarrow {}^7F_1$ transition is magnetic dipole allowed and independent of the local symmetry. The luminescence intensity ratio $I_{(J=2/J=1)}$ of the ${}^5D_0 \rightarrow {}^7F_2$ to ${}^5D_0 \rightarrow {}^7F_1$ is usually used to describe the degree of asymmetry in the vicinity of Eu^{3+} , and can thus provide valuable information about changes of the local structure around Eu^{3+} .^{39–42} As shown in Fig. 7, the intensity ratio $I_{(J=2/J=1)}$ decreases with increasing pressure up to 5 GPa, and can be associated with an increase in the average Eu-O bond distance or a decrease in the covalency of the Eu-O bond.⁴³ Above 5 GPa, $I_{(J=2/J=1)}$ increases continuously with elevated pressures up to the highest pressure of ~ 68 GPa, corresponding to the increase of the asymmetry of the dodecahedra induced by the application of pressure.

C. Raman spectroscopy

Figures 8(a) and 8(b) exhibit the pressure-induced evolutions of the Raman spectra and Raman frequencies for EGG.

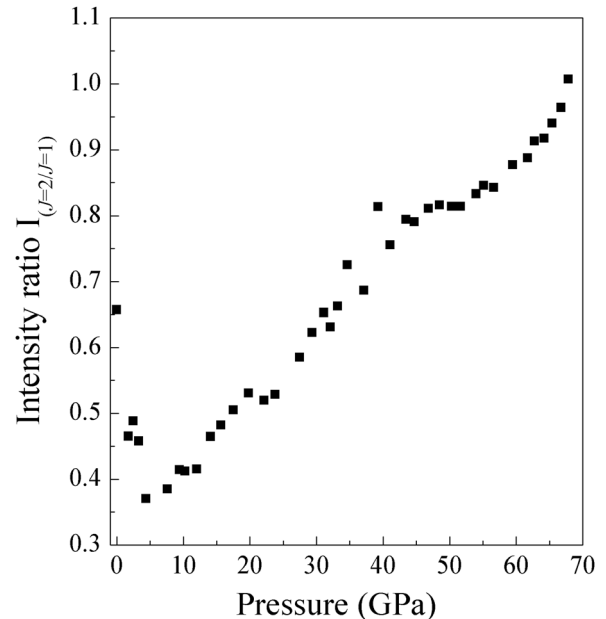


FIG. 7. Luminescence intensity ratio $I_{2/1}$ of the $I({}^5D_0 \rightarrow {}^7F_2)$ to $I({}^5D_0 \rightarrow {}^7F_1)$ transitions as a function of pressure.

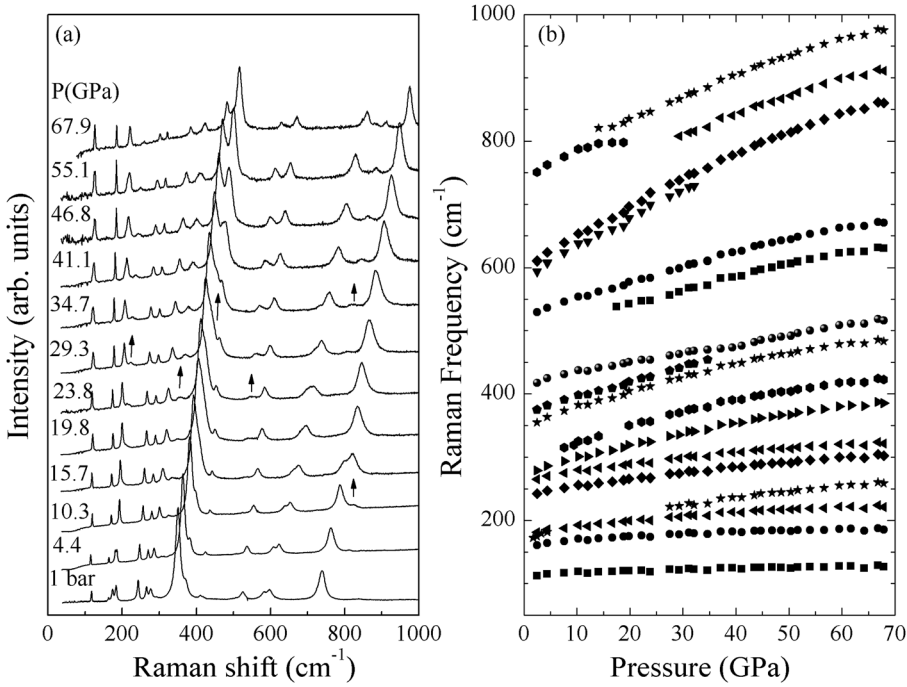


FIG. 8. Pressure evolution of (a) the Raman spectra of EGG and (b) the corresponding frequencies.

The symmetry assignments of the Raman modes have been reported earlier for $R_3Ga_5O_{12}$ ($R = Eu, Dy, Yb, Lu$).^{44–46} The frequencies at ambient pressure, symmetries, pressure coefficients, and mode Grüneisen parameters are tabulated in Table II. The pressure coefficients are obtained by the linear least-squares fitting procedure, while the mode Grüneisen parameters are calculated using the formula: $\gamma_i = (B_0/\omega_{0i})(d\omega_{0i}/dp)$, where ω_{0i} and B_0 are the ambient-pressure phonon

frequencies and the bulk modulus obtained from the Raman and x-ray diffraction data, respectively.

With increasing pressures, the Raman bands at low frequencies ($<170\text{ cm}^{-1}$) slightly shift to higher frequencies and increase in relative intensities (Fig. 8(a)). These bands correspond to the translational motion of the cations in the tetrahedral, octahedral, and dodecahedral sites.^{47,48} This indicates that the cationic sublattice retains its symmetry at least up to 68 GPa, which is in agreement with the results of the x-ray diffraction.

TABLE II. Derived vibrational parameters of $Eu_3Ga_5O_{12}$ from high-pressure Raman results. ω_0 : Raman frequency at ambient pressure; $d\omega_i/dP$: pressure derivative of the Raman frequency; γ_i : mode Grüneisen parameter.

$Eu_3Ga_5O_{12}$			
Symmetry	ω_0 (cm^{-1})	$d\omega_i/dP$ ($\text{cm}^{-1}/\text{GPa}$)	γ_i
E_g	112	0.17(1)	0.4
T_{2g}^2	158	0.26(2)	0.4
T_{2g}^2	168	1.01(3)	1.2
T_{2g}^2	178	0.52(2)	0.6
T_{2g}^2	237	0.83(2)	0.7
E_g	260	0.74(3)	0.5
T_{2g}^2	272	1.46(3)	1.1
E_g	289	1.57(5)	1.1
$A_{1g}^1 + E_g$	345	1.79(5)	1.0
T_{2g}^2	366	2.40(3)	1.3
T_{2g}^2	406	1.44(2)	0.7
E_g	414		
T_{2g}^2	505	1.92(4)	0.8
A_{1g}^1	520	2.08(4)	0.8
T_{2g}^2	577	4.19(9)	1.5
T_{2g}^2	592	3.56(7)	1.2
E_g	674	2.79(6)	0.8
A_{1g}^1	733	4.05(18)	1.1
T_{2g}^2	777	3.08(4)	0.8

On the other hand, new Raman bands appear and increase in the relative intensities with increasing pressures (arrows). Further analyses of these new Raman peaks show that they may have emerged from relatively lower pressures, or even ambient pressure, with enhanced intensities with increasing pressures—the intensities of these peaks may have been too weak to be observable at ambient conditions. Previous studies indicate that the Raman bands in the intermediate- and high-frequency regions ($>170\text{ cm}^{-1}$), to first approximate, can be assigned to the bending vibration and internal stretching of the tetrahedra GaO_4 .^{47,48} The change in the relative intensity of these peaks can be explained as a result of the lattice tilting and distortion of the GaO_4 tetrahedra. More especially, the high-frequency band at $\sim 738\text{ cm}^{-1}$ splits into two peaks at 10.3 GPa (Fig. 8(a)), and is accompanied by the change in the relative intensities with increasing pressure. Since the high-frequency bands higher than 738 cm^{-1} correspond to the internal stretching of the tetrahedra GaO_4 , the splitting is directly related to the deformation of GaO_4 . However, it should be noted that the GaO_4 tetrahedra are coupled with the GaO_6 octahedra through the corner-sharing oxygen atoms and the pressure-induced deformation of the tetrahedra is strongly linked with the change of the octahedra. As the Eu-O bond length is longer than the Ga-O bond, the changes in Raman spectra mainly correspond to the octahedral-tetrahedral

network, which is indicated by the Raman spectra and lattice dynamical calculation in $R_3Al_5O_{12}$.⁴⁷

Figure 8(b) shows the pressure dependence of the phonon frequencies for EGG. Generally, all of the phonon modes for EGG exhibit a positive response with increasing pressures in the pressure range of 0–67 GPa. The low frequency bands have small pressure coefficients. The high frequency modes with larger mean pressure coefficients are more sensitive to pressure than the intermediate and low frequency phonons.

IV. DISCUSSION

Combining the x-ray diffraction, PL, and Raman results at room temperature, here we discuss the crystal structural evolution of EGG under pressures. As indicated by the x-ray diffraction results, EGG retains the cubic garnet structure up to 75 GPa and mostly becomes amorphous at 85 GPa, which is consistent with that of GGG reported earlier.⁷ The cationic sublattices are insignificantly modified by the application of pressure until they collapse into an amorphous state since the x-ray diffraction technique is sensitive to cationic sublattices.

However, PL and Raman spectra in EGG reveal the pressure-induced significant modification of the local oxygen environment around the polyhedral sites. In the luminescence spectra of EGG, R1 and R2 lines corresponding to the ${}^5D_0 \rightarrow {}^7F_1$ transition of Eu^{3+} merge at 4.4 GPa. This is related to the decrease in the difference of the Eu-O bond lengths, associated with the pressure-induced lesser distortion of the dodecahedra EuO_8 . The decrease of the intensity ratio $I_{(J=2/J=1)}$ also implies the decrease of the asymmetry in the dodecahedral site which has been found in other REE garnets.^{25,49} In Nd^{3+} : GSGG, the fluorescence spectra imply that there is a tendency toward a cubic site symmetry for the dodecahedra in the pressure range of 0–12.6 GPa.²⁵ In Nd^{3+} : GGG, it has been found that the distances between the central Gd and all the surrounding oxygen ions become approximately equal to each other at ~ 11.8 GPa and the dodecahedra GdO_8 become less distorted.⁴⁹ Nevertheless, at the beginning of 7.6 GPa, the splitting of the 7F_2 sublevels of Eu^{3+} indicates onset of the opposite change of the crystal field around Eu^{3+} . Above 10 GPa, the peak broadening of the ${}^5D_0 \rightarrow {}^7F_2$ transition corresponding to the electric dipole is significantly modified by the application of pressure along with the appearance of the new Stark splittings at ~ 22.2 GPa and ~ 48.5 GPa. These changes are related to the shift of the oxygen atoms which leads to the increase of the disorder of the oxygen atoms around Eu^{3+} with increasing pressures. At ~ 68 GPa, the marked inhomogeneous distribution of the oxygen atoms surrounding the Eu^{3+} ion is suggested by the broad fluorescence spectra and the large intensity ratio $I_{(J=2/J=1)}$. The pressure-induced local structural disorder around the dodecahedral site has also been found in the fluorescence spectra of the Sm: YAG garnet¹⁰ and GSGG garnet doped with Nd^{3+} and Cr^{3+} .²⁵

Based on the analyses of the high-pressure Raman spectra, the appearance of the new Raman peaks cannot be attributed to the structural phase transition since EGG keeps its cubic garnet structure prior to the PIA transition shown by the x-ray diffraction. This can be explained as a result of the lattice tilting and distortion of the GaO_4 tetrahedra, as mentioned above. It should

be noted that this will be accompanied by the deformation of the GaO_6 octahedra since the tetrahedra are coupled with the octahedra due to the corner-sharing oxygen atoms. Papagelis *et al.* indicate that the force strength of the R-O bond in the REE garnets is much weaker than that of the tetrahedra and octahedra.⁴⁷ Therefore, the increase of the local oxygen environment around Eu^{3+} with increasing pressure can be viewed from the deformation of the tetrahedra and octahedra. On the other hand, the pressure forces the tetrahedra, octahedra, and dodecahedra to get closer to each other linearly with the shrinkage of the lattice constant (a) (inset of Fig. 5). For instance, one of the Ga_2 -Eu bonds between the dodecahedra and tetrahedra changes from ~ 3.09 Å at ambient pressure to ~ 2.85 Å at ~ 85 GPa. The shortening of the distances between polyhedra will lead to the repulsions and even overlapping of the polyhedra, accompanied by the deformation of the tetrahedra and octahedra and increase of the asymmetry in dodecahedral sites.

Considering the x-ray diffraction, Raman, and PL experimental results, here we propose that the amorphization of EGG results from the interaction and deformation of the tetrahedra, octahedra, and dodecahedra. When the cationic sublattices collapse into the disordered state, the overlapping of the tetrahedra and octahedra will occur due to the shortening of the distances between the polyhedra, resulting in the increase of the average coordination number of the Ga^{3+} ions. This mechanism has also been confirmed in the PIA transition of YIG, in which Gavriliuk *et al.*⁸ concluded that the local atomic structure in the amorphous state of YIG consists of the iron-oxygen FeO_6 octahedral complexes with disordered orientations of local axis and of other randomly arranged ion fragments with overall $Y_3Fe_5O_{12}$ composition.⁸

The PIA transition in EGG has some similarity with the compounds which have corner-sharing networks of tetrahedra and octahedra.^{3-5,17-20} For example, the PIA transition in ZrW_2O_8 ³ results from the rotation and tilting of tetrahedra WO_4 and octahedra ZrO_6 . However, the transition pressure of EGG (>50 GPa) is much higher than that of ZrW_2O_8 (<10 GPa). In the structure of ZrW_2O_8 , one oxygen of each WO_4 is bound to only one W atom, forming the flexible structure. This implies that the flexible octahedral-tetrahedral network in ZrW_2O_8 is sensitive to pressure, indicated by the softening of the low frequencies in the Raman spectra. Compared with this, REE cation inserts the octahedral-tetrahedral network in the structure of the REE garnets and is bonded to the oxygen atom which is shared by tetrahedron and octahedron (Fig. 1(b)). As a result, the REE cation will prevent the tiltings and distortions of the tetrahedra and octahedra when pressure is applied. Therefore, REE cations which support the octahedral-tetrahedral network plays an important role in the structural stability of the REE garnet.

Hua *et al.* proposed the decomposition path of $Gd_3Sc_2Ga_3O_{12} \rightarrow 3GdGaO_3 + Sc_2O_3$ in GSGG to explain the thermodynamics and driving mechanism of the crystalline-to-amorphous transition.^{7,25} This is favored by the fact that some synthetic garnets such as YIG and YAG may undergo decomposition at moderately high P - T conditions.²⁶ However, we observed garnet-to-perovskite phase transition in GSGG at 24 GPa and 1500–2000 K in the earlier work,²⁹ rather than the decomposition. For EGG, the laser-heating experiment

confirmed the garnet-to-perovskite transition at high P - T conditions (Fig. 4), which is consistent with GSGG. The garnet-to-orthorhombic phase transition has also been observed in the silicate garnets such as grossular ($\text{Ca}_3\text{Al}_2\text{Si}_3\text{O}_{12}$) and pyrope ($\text{Mg}_3\text{Al}_2\text{Si}_3\text{O}_{12}$) at high P - T conditions.^{50–55} Recently, the amorphous GGG and YIG have been reported to transform to a single cubic or orthorhombic perovskite structure at high P - T conditions.^{27,28} Based on these results, we conclude that the PIA transition in EGG is kinetically hindered and the amorphization is a new thermodynamic state resulting from the hindrance of a crystal-to-crystal phase transition.

V. CONCLUSIONS

In summary, the tetrahedra and octahedra in the corner-sharing network of EGG become distorted with increasing pressures, leading to the marked inhomogeneous distribution of the oxygen atoms around the dodecahedral sites. The interaction and deformation of the polyhedra under high pressures induce the PIA transition of EGG at 85 GPa. In the amorphous state, the tetrahedra and octahedra are overlapped with each other, resulting in the increase of the average coordinate numbers. Our laser-heated DAC experiment confirmed that the PIA transition for EGG results from the kinetic hindrance of a crystal-to-crystal phase transition.

ACKNOWLEDGMENTS

Financial supports from the National Natural Science Foundation of China (Grant No. 11079040) and the National Basic Research Program of China (2011CB808200) are gratefully acknowledged. The experimental work was performed at 4W2 beamline of BSRF, which was supported by the Chinese Academy of Sciences (Grant Nos. KJCX2-SW-N20 and KJCX2-SW-N03). This work at UT Austin was supported as part of EFree, an Energy Frontier Research Center funded by the U.S. Department of Energy office of Science, Office of Basic Energy Sciences under Award No. DE-SC0001057. We also thank N. Seymour and L. Dafov for editing the manuscript.

- ¹R. J. Hemley, A. P. Jephcoat, H. K. Mao, L. C. Ming, and M. H. Manghnani, *Nature* **334**, 52 (1988).
- ²P. Gillet, J. Badro, B. Varrel, and P. F. Mcmillan, *Phys. Rev. B* **51**, 11262 (1995).
- ³C. A. Perottoni and J. A. H. da Jornada, *Science* **280**, 886 (1998).
- ⁴W. Paraguassu, M. Maczka, A. G. Souza, P. T. C. Freire, J. Mendes, and J. Hanuza, *Phys. Rev. B* **82**, 174110 (2010).
- ⁵O. L. Bacq, D. Machon, D. Testemale, and A. Pasturel, *Phys. Rev. B* **83**, 214101 (2011).
- ⁶O. Mishima, L. D. Calvert, and E. Whalley, *Nature* **310**, 393 (1984).
- ⁷H. Hua, S. Mirov, and Y. K. Vohra, *Phys. Rev. B* **54**, 6200 (1996).
- ⁸A. G. Gavriliuk, V. V. Struzhkin, I. S. Lyubutin, M. I. Erements, I. A. Trojan, and V. V. Artemov, *JETP Lett.* **83**, 37 (2006).
- ⁹J. Liu and Y. K. Vohra, *Solid State Commun.* **88**, 417 (1993).
- ¹⁰J. Liu and Y. K. Vohra, *Appl. Phys. Lett.* **64**, 3386 (1994).
- ¹¹J. Liu and Y. K. Vohra, *J. Appl. Phys.* **79**, 7978 (1996).
- ¹²S. Kobyakov, A. Kamińska, A. Suchocki, D. Galanciak, and M. Malinowski, *Appl. Phys. Lett.* **88**, 234102 (2006).
- ¹³U. Hömmerich and K. L. Bray, *Phys. Rev. B* **51**, 12133 (1995).
- ¹⁴Y. R. Shen and K. L. Bray, *Phys. Rev. B* **56**, 10882 (1997).
- ¹⁵A. Kamińska, S. Biernacki, S. Kobyakov, A. Suchocki, G. Boulon, M. O. Ramirez, and L. Bausa, *Phys. Rev. B* **75**, 174111 (2007).
- ¹⁶D. Galanciak, M. Grinberg, W. Gryk, S. Kobyakov, A. Suchocki, G. Boulon, and A. Brenier, *J. Phys.: Condens. Matter* **17**, 7185 (2005).

- ¹⁷T. Varga and A. P. Wilkinson, *Phys. Rev. B* **79**, 224119 (2009).
- ¹⁸W. Paraguassu, M. Maczka, A. G. S. Filho, P. T. C. Freire, J. M. Filho, F. E. A. Melo, L. Macalik, L. Gerward, J. S. Olsen, A. Waskowska, and J. Hanuza, *Phys. Rev. B* **69**, 094111 (2004).
- ¹⁹N. Garg, C. Murli, A. K. Tyagi, and S. M. Sharma, *Phys. Rev. B* **72**, 064106 (2005).
- ²⁰T. Sakuntala, A. K. Arora, V. Sivasubramanian, R. Rao, S. Kalavathi, and S. K. Deb, *Phys. Rev. B* **75**, 174119 (2007).
- ²¹D. A. Keen, A. L. Goodwin, M. G. Tucker, M. T. Dove, J. S. O. Evans, W. A. Crichton, and M. Brunelli, *Phys. Rev. Lett.* **98**, 225501 (2007).
- ²²C. A. Figueiredo, J. Catafesta, J. E. Zorzi, L. Salvador, I. J. R. Baumvol, M. R. Gallas, J. A. H. da Jornada, and C. A. Perottoni, *Phys. Rev. B* **76**, 184201 (2007).
- ²³A. K. Arora, *Solid State Commun.* **115**, 665 (2000).
- ²⁴G. Lucazeau, P. Bouvier, A. Pasturel, O. L. Bacq, and T. Pagnier, *Acta Phys. Pol. A* **116**, 25 (2009).
- ²⁵H. Hua, J. Liu, and Y. K. Vohra, *J. Phys.: Condens. Matter* **8**, L139 (1996).
- ²⁶M. Marezio, J. P. Remeika, and A. Jayarama, *J. Chem. Phys.* **45**, 1821 (1966).
- ²⁷Z. Mao, S. M. Dorfman, S. R. Shieh, J. F. Lin, V. B. Prakapenka, Y. Meng, and T. S. Duffy, *Phys. Rev. B* **83**, 054114 (2011).
- ²⁸J. Wang, Z. Mao, S. M. Dorfman, V. B. Prakapenka, and T. S. Duffy, *Fall Meet. Suppl. EOS Trans. AGU* **90**, Abstract MR13A (2009). Available at <http://adsabs.harvard.edu/abs/2009AGUFMMR13A1670W>.
- ²⁹C. Lin, J. Liu, J. F. Lin, X. Li, Y. Li, Q. Zhang, L. Xiong, and R. Li, *Inorg. Chem.* **52**, 431 (2013).
- ³⁰J. C. Kim, M.-H. Kim, J.-B. Lim, and S. Nahm, *J. Am. Ceram. Soc.* **90**, 641 (2007).
- ³¹N. C. Holmes, J. A. Moriarty, G. R. Gathers, and W. J. Nellis, *J. Appl. Phys.* **66**, 2962 (1989).
- ³²H. K. Mao, J. Xu, and P. M. Bell, *J. Geophys. Res., [Solid Earth]* **91**, 4673, doi:10.1029/JB091iB05p04673 (1986).
- ³³J. Hammersley, *Fit2d User Manual* (Grenoble: ESRF), 1996.
- ³⁴B. H. Toby, *J. Appl. Crystallogr.* **34**, 210 (2001).
- ³⁵A. Boulif and D. Louer, *J. Appl. Crystallogr.* **37**, 724 (2004).
- ³⁶F. Birch, *J. Geophys. Res.* **83**, 1257, doi:10.1029/JB083iB03p01257 (1978).
- ³⁷V. V. Valiev, J. B. Gruber, D. J. Fu, V. O. Pelenovich, G. W. Burdick, and M. E. Malysheva, *J. Rare Earths* **29**, 776 (2011).
- ³⁸J. B. Gruber, U. V. Valiev, G. W. Burdick, S. A. Rakhimov, M. Pokhrel, and D. K. Sardar, *J. Lumin.* **131**, 1945 (2011).
- ³⁹G. Chen, R. G. Haire, and J. R. Peterson, *J. Phys. Chem. Solids* **56**, 1095 (1995).
- ⁴⁰D. Machon, V. P. Dmitriev, V. V. Sinityn, and G. Lucazeau, *Phys. Rev. B* **70**, 094117 (2004).
- ⁴¹R. Praveena, V. Venkatramu, P. Babu, C. K. Jayasankar, T. Troster, W. Sievers, and G. Wortmann, *J. Phys.: Conf. Ser.* **121**, 042015 (2008).
- ⁴²Q. G. Zeng, Z. J. Ding, Z. M. Zhang, and Y. Q. Sheng, *J. Phys. Chem. C* **114**, 4895 (2010).
- ⁴³J. A. Capobianco, P. P. Proulx, M. Bettinelli, and F. Negrisolo, *Phys. Rev. B* **42**, 5936 (1990).
- ⁴⁴J. J. Song, P. B. Klein, R. L. Wadsack, M. Selders, S. Mroczkow, and R. K. Chang, *J. Opt. Soc. Am.* **63**, 1135 (1973).
- ⁴⁵R. L. Wadsack, J. L. Lewis, B. E. Argyle, and R. K. Chang, *Phys. Rev. B* **3**, 4342 (1971).
- ⁴⁶R. C. Middleton, D. V. S. Muthu, and M. B. Kruger, *Solid State Commun.* **148**, 310 (2008).
- ⁴⁷K. Papagelis, G. Kanellis, S. Ves, and G. A. Kourouklis, *Phys. Status Solidi B* **233**, 134 (2002).
- ⁴⁸P. Gillet, G. Fiquet, J. M. Malezieux, and C. A. Geiger, *Eur. J. Mineral.* **4**, 651 (1992). Available at <http://eurjmin.geoscienceworld.org/content/4/4/651.full.pdf+html>.
- ⁴⁹A. Kaminska, R. Buczek, W. Paszkowicz, H. Przybylińska, E. Werner-Malento, A. Suchocki, M. Brik., A. Durygin, V. Drozd, and S. Saxena, *Phys. Rev. B* **84**, 075483 (2011).
- ⁵⁰H. Yusa, T. Yagi, and N. Shimobayashi, *Phys. Earth Planet. Inter.* **92**, 25 (1995).
- ⁵¹S. Greaux, N. Nishiyama, Y. Kono, L. Gautron, H. Ohfujii, T. Kunimoto, N. Menguy, and T. Irifune, *Phys. Earth Planet. Inter.* **185**, 89 (2011).
- ⁵²T. Irifune, T. Koizumi, and I. J. Ando, *Phys. Earth Planet. Inter.* **96**, 147 (1996).
- ⁵³E. Ito, A. Kubo, T. Katsura, M. Akaogi, and T. Fujita, *Geophys. Res. Lett.* **25**, 821 (1998).
- ⁵⁴J. M. Walter, A. Kubo, T. Yoshino, J. Brodholt, T. K. Koga, and Y. Ohishi, *Earth Planet. Sci. Lett.* **222**, 501 (2004).
- ⁵⁵S. Tateno, K. Hirose, N. Sata, and Y. Ohishi, *Geophys. Res. Lett.* **32**, L15306, doi:10.1029/2005GL023309 (2005).